DOI 10.1007/s11595-017-1706-7

Crystallization and Luminescence Properties of Sm^{3+}-Doped $SrO\text{-}Al_2O_3\text{-}SiO_2$ Glass-Ceramics

LI Hong[1], LIU Liwang[1], TANG Xiaozhe[1], WANG Qian[1], Paul W Wang[2], WANG Wei[3,4,5*]

(1. State Key Laboratory of Silicate Materials for Architectures (Wuhan University of Technology), Wuhan 430070, China; 2. Department of Physics, Bradley University, Peoria 10, 61625, USA; 3.School of Automotive Engineering, Wuhan University of Technology, Wuhan 430070, China; 4.Hubei Province Key Laboratory of Modern Automotive Technology, Wuhan 430070, China; 5.Hubei Province Automotive Parts Synergy Innovation Center, Wuhan 430070, China)

Abstract: The Sm^{3+}-doped $SrO\text{-}Al_2O_3\text{-}SiO_2$ (SAS) glass-ceramics with excellent luminescence properties were prepared by batch melting and heat treatment. The crystallization behavior and luminescent properties of the glass-ceramics were investigated by DTA, XRD, SEM and luminescence spectroscopy. The results indicate that the crystal phase precipitated in this system is monocelsian ($SrAl_2Si_2O_8$) and with the increase of nucleation/crystallization temperature, the crystallite increases from 66 % to 79 %. The Sm^{3+}-doped SAS glass-ceramics emit green, orange and red lights centered at 565, 605, 650 and 715 nm under the excitation of 475 nm blue light which can be assigned to the $^4G_{5/2}\rightarrow{}^6H_{j/2}$ (j=5, 7, 9, 11) transitions of Sm^{3+}, respectively. Besides, by increasing the crystallization temperature or the concentration of Sm^{3+}, the emission lights of the samples located at 565, 605 and 650 nm are intensified significantly. The present results demonstrate that the Sm^{3+}-doped SAS glass-ceramics are promising luminescence materials for white LED devices by fine controlling and combining of these three green, orange and red lights in appropriate proportion.

Key words: Sm^{3+}-doped; $SrO\text{-}Al_2O_3\text{-}SiO_2$; glass-ceramic; crystallization; luminescence properties

1 Introduction

White light-emitting diodes (LEDs) which have been improved greatly in recent years are being applied to many commercial areas such as traffic lights, mobile phones, special lighting, and display units. The application of LEDs will continue to expand, eventually to the field of general lighting. In comparison with incandescent and fluorescent lamps, the InGaN-based LEDs have many designable features such as high quantum efficiency, long lifetime, and compactness[1-6]. There is no doubt that the white LED lighting has a profound effect on the lighting industry and will change the conventional lighting. Currently, the white light can be created in two approaches: mixed-color white light[7,8] and phosphor-converted white light[9-14]. The first approach is to mix different lights from corresponding LED that displays white light. Similarly, the so-called tri-phosphor fluorescent lamps use three kinds of phosphors. When the phosphors are under the ultraviolet radiation from the mercury arc in the lamp tube, they emit a relatively narrow spectrum of blue, green, and red light. By mixing appropriate amount of their output, the obtained light is white in appearance. The other approach to create white light is by using mix-color (YAG) phosphor together with a GaN blue LED chip (450-470 nm). When some of phosphors in the LED are excited by blue light, they emit yellow light with a broad spectrum. Some of the blue light will be converted to yellow light by phosphor, the remaining blue light, when mixed with the yellow light, results in white light. For the mixed-color white LED, the color temperature of RGB LEDs is instable because of the degradation or variation of driving current. Besides, different color LED requires different driving currents, complicating their fabrication and structure[15].

Hence, the current leading commercial white light is created by using the phosphor-converted approach. It normally uses a 450-470 nm GaN chip coated by yellow phosphor, which is made of $Y_3Al_5O_{12}:Ce^{3+}$ (Ce:YAG) usually. Matrix materials essentially homogeneously disperse phosphors and keep the formation on the blue GaN chip. So far, the curable silicone is the most widely used matrix materials in the wavelength converters for phosphors for their low fabricating cost and excellent optical transmittance.

(Received: Oct. 20, 2016; Accepted: June 4, 2017)

LI Hong(李宏): Prof.; Ph D; E-mail: lh_648@whut.edu.cn

*Corresponding author: WANG Wei(王伟): Ph D; Assoc. Prof.; E-mail: 1542322682@qq.com

Funded by the National Natural Science Foundation of China (No.5137217), Hubei Province Foreign Science and Technology Project (No.2016AHB027) and Science and Technology Planning Project of Hubei Province (No.2014BAA136)

However, problem still exists: because of the low glass transition temperature, the mthy1 groups are usually detached from silicon under the radiation from the LED after a period of operation[16]. That makes the curable silicone turns yellow and consequently decreases the transmittance of the wavelength converters. Furthermore, the yellowish silicone results in luminescent loss and chromaticity shift[17,18]. Therefore, it is of significance to develop novel and durable material to server as an alternative way of using the curable silicone, especially in the application where high power LEDs are essentially required. The glass-ceramics, as innovative luminescent materials, combining with glass and crystals, have drawn numerous attention for their excellent luminescence properties, machinability and high uniformity and stability[19-21]. Moreover, with the rapid development in recent years, the conventional silicone-based phosphor converter has been successfully replaced for fabrication high power white LED[22-26]. In numerous glass-ceramic systems, silicate system is one of the best choices for its good thermal stability and physicochemical property. Recently, the studies on Tb, Dy and Sm are becoming much more significant because of their extensive application in the field of lasers, optical communications, solid-phase optical transmitters and up/down conversion[27]. Among these ions, Sm^{3+} is one of the promising activators in many glass matrixes with efficient emissions from visible region to near-infrared region. That is ascribed to the high quantum efficiency of the $^4G_{5/2}$ and its multifarious radiative emission paths, shown in Fig.1. These amazing features make it favored in the application of medical diagnostics[28], color displays[29] and white LEDs[30].

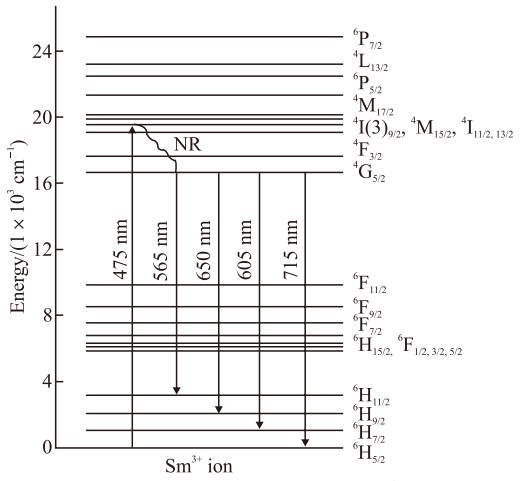

Fig. 1 Energy level diagram of Sm^{3+} ions

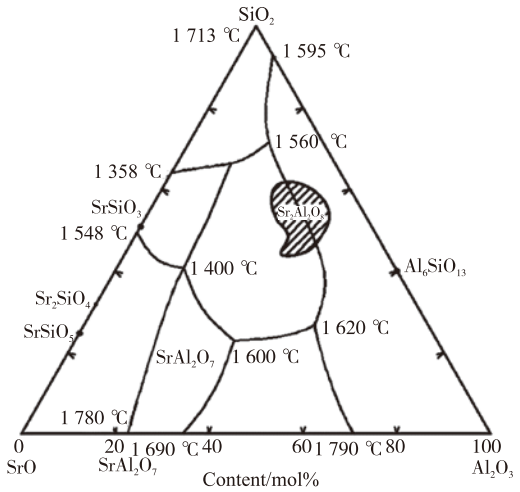

Fig. 2 Ternary phase diagrams of SrO-Al_2O_3-SiO_2

In this paper, 27SrO-19Al_2O-41.5SiO_2-2CaO-3MgO-3B_2O_3-3TiO_2-1ZrO-0.5Sb_2O_3 (SAS) was chosen for its relatively high crystallinity based on our previous work[31]. And the crystallization and luminescence properties of Sm^{3+}-doped SAS glass-ceramics with different heat treatment schedules and different Sm^{3+}-contents were investigated. According to the ternary phase diagrams of SrO-Al_2O_3-SiO_2 showed in Fig.2, we chose the composition of the matrix glass corresponding to the eutectic point. Finally, based on the thermal analysis, we chose the treatment schedule of the samples. Our results manifested that the composition and heat treatment schedule are the crucial factors to tailor the properties of the glass and its counterpart glass ceramics. This Sm^{3+} doped glass ceramic may be a promising candidate for white LED device.

2 Experimental

Sm^{3+}-doped glasses with the composition of 27SrO -19Al_2O_3 -41.5SiO_2 -2CaO-3MgO-3B_2O_3-3TiO_2-1ZrO-0.5Sb_2O_3-(0.05-0.15) Sm_2O_3 (mol %) were prepared by the raw reagent grade materials such as $SrCO_3$, Al_2O_3, SiO_2, $CaCO_3$, MgO, H_3BO_3 and Sm_2O_3. About 100 g batch materials were homogeneously milled and mixed for 1 h. Then the mixture was transferred into a 150 mL corundum crucible and heated in a furnace. The furnace was heated up at a rate of 3 ℃/min from room temperature to 1 550 ℃, and then kept at this temperature for 2 h. Blocks of bulk transparent glasses were produced by casting melts onto a preheated steel mold and then immediately annealing at 600 ℃ for 1 h to release the inner stress and thermal strains and then cooling slowly to room temperature inside the furnace. The bulk glasses were

Table 1 Heat treatment schedule and Sm^{3+} contents in the samples

Samples	Nucleation temperature/℃	Nucleation time/h	Crystallization temperature/℃	Crystallization time/h	Sm^{3+}-content/(mol%)
C1	850	3	1 050	3	0.10
C2	900	3	1 050	3	0.10
D0	950	3	1 050	3	0.10
D1	950	3	1 100	3	0.10
D2	950	3	1 150	3	0.10
E0	950	3	1 100	3	0.05
E1	950	3	1 100	3	0.15

subjected to heat treatment in accordance with the DTA characteristic temperature data obtained from DTA machine with model number NETZSCH STA 449, Germany.

Finally, a two-step heat treatment was applied which involved heat treatment at a temperature in the vicinity of T_g to produce a high density of crystal nuclei, followed by treatment between 1 050 and 1 150 ℃ to grow the nuclei. This procedure is crucial to generate much more and smaller crystallites compared with the single-step heat treatment. The heat treatment schedules of samples are listed in Table 1. All the samples were processed into plates of about 20 × 10 × 2 mm in size for measurement.

The crystalline phases were identified by using an X-ray diffractometer (RIGAKUD/Max-RB, Japan). The morphology of the glass-ceramics was observed by using a scanning electron microscope (SEM, JEOL JSM-5610LV, Japan) with 20 kV accelerating voltage. Emission and excitation spectra of the samples were recorded at room temperature with a luminescence spectrophotometer (Jasco FP-6500, China).

3 Results and discussion

3.1 Differential thermal analysis

The DTA data together with the characteristic temperature are reported in Fig.3. It is demonstrated that the glass transition occurs at around 767 ℃ and the exothermic peak locates at 937 ℃, which is consistent with the crystallization peak temperature in literature[32].

3.2 Crystallization properties

The X-ray diffraction patterns in Fig.4 show that all the diffraction peaks of the samples are located at the same positions. These diffraction peaks are well-matched with the standard powder diffraction data 38-1454, which reveal the formation of $SrAl_2Si_2O_8$ crystals in all the samples. It is indicated that the crystal structure has not been changed though the Sm^{3+} ions occupy the sites of Sr^{2+} within $SrAl_2Si_2O_8$ because of the nearly matched ionic size of Sm^{3+} (96.4 pm) and Sr^{2+} (113 pm). Comparing the intensities of diffraction peaks in Figs.4 (a) and (b), both the nucleation temperature and the crystallization temperature have an impact on the crystallization process. But the diffraction intensities show little change with increasing nucleation temperature from 850 to 950 ℃. However, when the crystallization temperature increases from 1 050 to 1 150 ℃, the diffraction intensities are significantly enhanced, especially in sample D2. This can be explained as follows: at the first stage of heat treatment, the major process is the formation of crystal seeds, and a mass of small-sized nuclei are formed in this period. But at the second stage, the nuclei are dramatically growing up. So the crystallization temperature plays a major role in crystallization. The higher the crystallization temperature, the larger volume fraction of crystal phases.

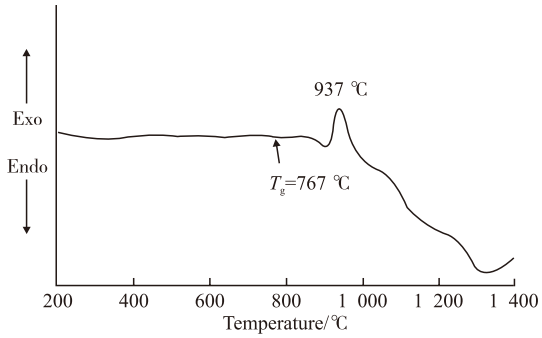

Fig.3 DTA scan curve of SAS glass powder (The glass samples are held in an alumina crucible and analyzed by taking the highly purified Al_2O_3 powder as reference at a heating rate of 10 ℃/min from room temperature to 1 400 ℃)

Furthermore, the scanning electron micrographs of etched surfaces of the glass-ceramic samples showed in Fig.5 reveal a clear morphology of grains with an average size ranging from 0.1 to 0.3 μm, whereas samples D1 and D2 show greater sizes ranging from 0.4 to 0.5 μm. That demonstrates that the crystallization temperature is a dominant factor for the precipitation crystallites and a higher nucleation temperature or crystallization temperature accelerates the formation

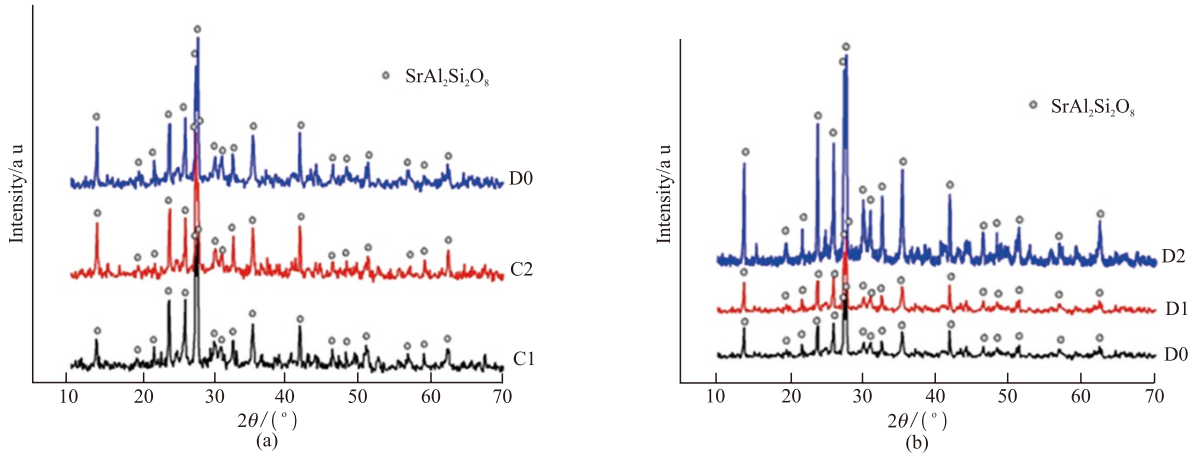

Fig.4 X-ray diffractograms of Sm^{3+} doped SAS glass-ceramics: (a) after different nucleation temperature treatments; and (b) after various crystallization temperature treatments (The measurements are conducted with 2θ from 10^{o} to 80^{o} by using Cu Kα_1 as radiation source)

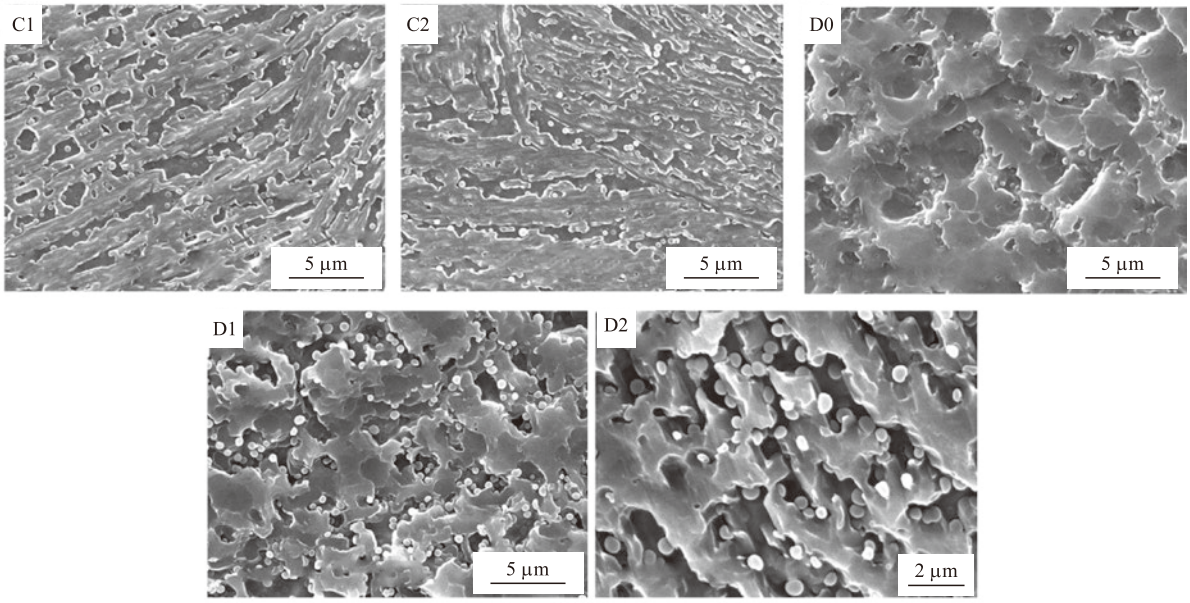

Fig.5 SEM images of the samples after various heat treatment schedules

of $SrAl_2Si_2O_8$ phase. Comparing the micrographs taken from the samples reveals structural difference, and it is apparent that this micro structural difference can be attributed to the large grain size and densification of structure of D1 and D2 compared to that of the C1 and C2.

The crystallinity of the samples is estimated from XRD diffraction peaks by using MDI Jade 5.0 software. The first three data points in Fig.6 show the nucleation temperature effect on the crystallinity ratios while the crystallization temperature is kept at 1 050 ℃. It is obvious that the crystallinity ratios increase from 66 % to 77 %. The ratio increases dramatically during the first 50 ℃ increase in temperature than during the second 50 ℃ increase. The last three data points in Fig.6 show the crystallization temperature effect on the crystallinity ratios while the nucleation temperature is kept at 950 ℃. It is shown that the crystallinity ratios increase from 77 % to 79 %. The increase rate of the crystallinity ratio is a little faster during the first 50 ℃ increase in crystallization temperature than during the second 50 ℃ increase.

Results of micrographs (Fig. 5) and crystallization ratios calculation (Fig. 6) show that the microstructures of glass-ceramics and size of grains (samples C1 and C2) have no significant change when the nucleation temperature changes from 850 to 900 ℃, and the formation of crystal seed other than growth of crystal is the major procedure in this process. However, with increasing nucleation temperature from 900 to 950 ℃ as in the case of sample D0, the micrograph changes significantly. This is the reason why the temperature of

950 ℃ is chosen to investigate how the crystallization temperature affects the crystal size and crystallinity.

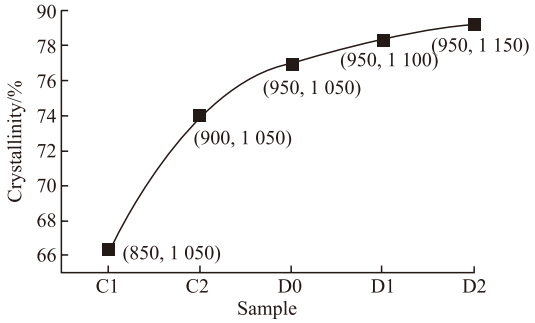

Fig.6 Dependence of crystallinity on the heat treatment schedules (The temperatures in the paraphrases in ℃ represent nucleation temperature and crystallization temperature, respectively)

3.3 Luminescence properties

The luminescence spectra of C0-C2, D0-D2 samples at room temperature are showed in Fig.7. The excitation spectra of Sm^{3+}-doped SAS glass-ceramics obtained by monitoring the emission at 600 nm are shown in Fig.7(a). Three broad excitation bands centered at 405, 440 (relatively weak) and 475 nm are observed and they are assigned to the transition from the ground state to $^6P_{2/3}$, $^4M_{17/2}$ and $^4I_{11/2,\ 13/2}$ or $^4M_{15/2}$, respectively[33]. In the excitation spectra, the luminous intensities of glass-ceramics (samples C1, C2, D0-D2) are obviously enhanced than that of the corresponding glass (sample C0) without any heat treatment), and the excitation peak and emission intensities of these glass-ceramics increase as the nucleation/crystallization temperature increases. The intensity is more obviously affected by the crystallization temperature than the nucleation temperature. Besides, the heat treatments did not change the locations of the excitation peaks, but affected the luminescent intensity.

The emission spectra of C0-C2 and D0-D2 samples excited by 475 nm are shown in Fig.7(b). As shown in the spectra, the specimen without heat treatment (sample C0) produces the weakest emission than those after the heat treatments. It has also been noticed that the emission intensities of samples C1 and C2 emitted at 565, 605, and 650 nm are similar, which is probably due to the similar structure of C1 and C2 as shown in Fig.5. Furthermore, the emission peaks located at 565, 605 and 650 nm are enhanced significantly when the crystallization temperature increases (samples D0, D1, and D2). The reason for the enhanced emission may be attributed to the following two aspects: firstly, the higher crystallization temperature leading to the higher crystallinity of

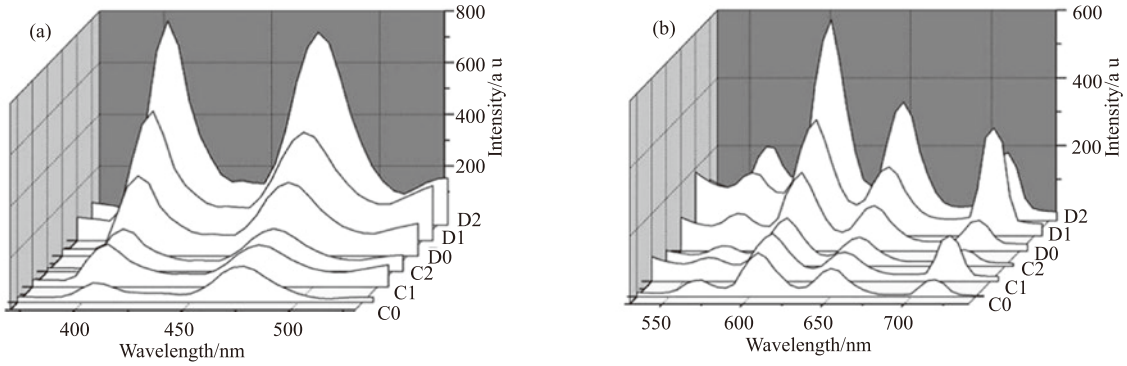

Fig.7 Luminescence spectra of the samples after different heat treatment: (a) Excitation spectra obtained by monitoring the emission at 600 nm wavelength; (b) Emission spectra obtained by exciting with 475 nm wavelength

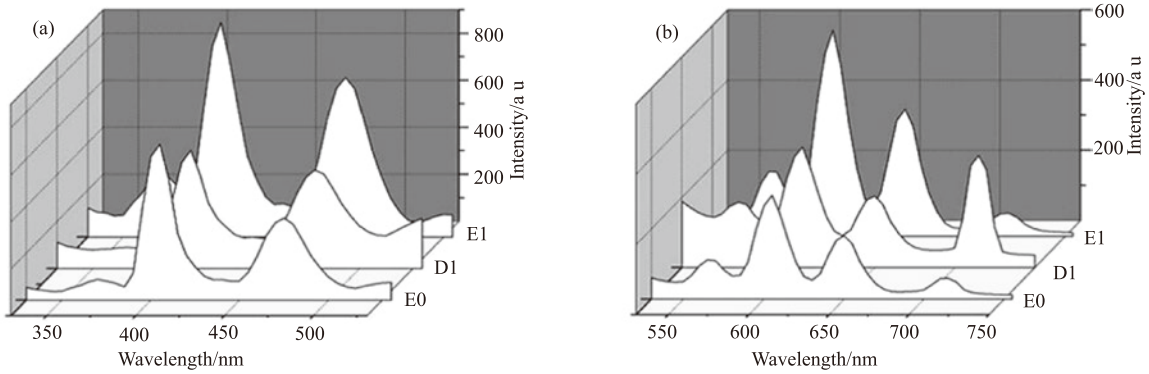

Fig.8 Luminescence spectra of the samples with different Sm^{3+} contents (E0 0.05 mol %, D1 0.10 mol %, E1 0.15 mol %): (a) Excitation spectra obtained by monitoring the emission at 600 nm wavelength; (b) Emission spectra obtained by exciting with 475 nm wavelength

$SrAl_2Si_2O_8$ phase in the sample which decreases defects in glass and thus reduces non-radiative relaxation[20,34]; secondly, the larger ratio of $SrAl_2Si_2O_8$ may reduce the effective phonon energy[35]. As we know, the wave number of high-energy phonon is about 1 000 cm^{-1} for the silicate oxide glass which is much lower in the corresponding crystal[36]. After the heat treatment, some of the Sm^{3+} ions are incorporated into the precipitated $SrAl_2Si_2O_8$ crystal lattice and replace the Sr^{2+} sites. The effective phonon energy coupled to Sm^{3+} ions is therefore reduced from that of high-energy phonon in SrO-Al_2O_3-SiO_2 glass to that of low-energy phonon in monocelsian crystals. Therefore, the replacement of Sm^{3+} for Sr^{2+} can reduce the probabilities of the multi-phonon relaxation and non-radiative transition, resulting in an enhanced luminescence. However, the tendency of peaks' intensities centered at 715 nm is not obvious, this is because the emission of Sm^{3+} at 715 nm is very feeble[37-39], which may make the appearance intensity at 715 nm very susceptible to the emission of host glass and the surrounding environment of Sm^{3+}.

The excitation and emission spectra of Sm^{3+}-doped SAS glass-ceramics with various Sm^{3+} contents are shown in Fig.8. Similar to the spectra in Fig.7, the location of the excitation wavelength peaks is independent to the contents of Sm^{3+} in the samples, but the contents of Sm^{3+} in the samples did affect the luminescent intensities. For D1 and E1, more Sm^{3+} ions are incorporated into the precipitated $SrAl_2Si_2O_8$ crystal lattice to act as luminous center resulting in the enhanced emission peaks at 565, 605 and 650 nm, and the emission peak located at 715 nm shows no specific trends, which is because the emission at 715 nm is very susceptible to the emission of host glass and the surrounding environment of Sm^{3+}, as has been explained above.

The tendency of emission intensities is very similar to that of the samples with different heat treatment temperatures: when the concentration of Sm^{3+} increases from 0.05 mol % to 0.15 mol %, the emission intensities located at 565, 605 and 650 nm are increased correspondingly.

4 Conclusions

This study shows that Sm^{3+}-doped SAS glass-ceramics emit green, orange and red lights located at 565, 605, 650 and 715 nm under the excitation of 475 nm laser. With increasing heat treatment temperature, the crystallinity is increased from 66 % to 79 % in this experiment. The crystallization temperature has a significant impact on crystallization and luminescent intensity than the nucleation temperature. As the crystallization temperature increases, the crystallinity and the light-emitting centered at 565, 605 and 650 nm become higher because the Sm^{3+} ions are incorporated into the precipitated $SrAl_2Si_2O_8$ crystal. Besides, with increasing concentration of Sm^{3+} from 0.05 mol % to 0.15 mol %, the intensity is also enhanced. Therefore, the intensity ratios of these emission peaks could be adjusted by fine tuning the heat treatment schedules of glass-ceramics and contents of Sm^{3+} ions. We envision that the Sm^{3+}-doped SAS glass-ceramics are promising luminescence materials for white LED devices by the combining of these green, orange and red lights in justified proportion.

References

[1] Ju G, Hu Y, Chen L, *et al.* A Reddish Orange-Emitting Stoichiometric Phosphor $K_3Eu(PO_4)_2$ for White Light-Emitting Diodes[J]. *Opt. Laser Technol.*, 2012, 44(1): 39-42

[2] Korthout K, Smet P F and Poelman D. Rare Earth Doped Core-Shell Particles as Phosphor for Warm-White Light-Emitting Diodes[J]. *Appl. Phys. Lett.*, 2011, 98(26): 261 919

[3] Narukawa Y. White-Light LEDs[J]. *Opt. Photonics News*, 2004, 15(4): 24-29

[4] Park W, Song Y, Moon J, *et al.* Synthesis and Luminescent Properties of Eu^{2+} Doped Nitrogen-Rich Ca-α-SiAlON Phosphor for White Light-Emitting Diodes[J]. *Solid State Sci.*, 2010, 12(11): 1 853-1 856

[5] El-Ghoroury H S, Yeh M, Chen J, *et al.* Growth of Monolithic Full-Color Gan-Based LED with Intermediate Carrier Blocking Layers[J]. *AIP Adv.*, 2016, 6(7): 075 316

[6] Iida D, Lu S, Hirahara S, *et al.* Enhanced Light Output Power of Ingan-Based Amber LEDs by Strain-Compensating AlN/AlGaN Barriers[J]. *J. Cryst. Growth*, 2016: 448 105-448 108

[7] Chen D, Xiang W, Liang X, *et al*. Advances in Transparent Glass–Ceramic Phosphors for White Light-Emitting Diodes-a Review[J]. *J. Eur. Ceram. Soc.*, 2015, 35(3): 859-869

[8] Kido J, Kimura M and Nagai K. Multilayer White Light-Emitting Organic Electroluminescent Device[J]. *Science*, 1995, 267(5 202): 1 332

[9] Gong M, Liang X, Wang Y, *et al*. Novel Synthesis and Optical Characterization of Phosphor-Converted WLED Employing Ce: YAG-Doped Glass[J]. *J. Alloys Compd.*, 2016, 664 125-664 132

[10] Fan J, Qian C, Zhang M, *et al.* Thermal, Optical and Electrical Analysis on Phosphor-Converted White LED Chip Scale Packages with Both Experiment and Simulation[C]. *2016 17th International Conference on Thermal, Mechanical and Multi-Physics Simulation and Experiments in Microelectronics and Microsystems (EuroSimE)*, 2016

[11] Zhao Y, Xu H, Zhang X, *et al.* Facile Synthesis of YAG: Ce^{3+} Thick

Films for Phosphor Converted White Light Emitting Diodes[J]. *J. Eur. Ceram. Soc.*, 2015, 35(13): 3 761-3 764

[12] Chen Z, Zhang J, Chen S, *et al*. Preparation and Luminescence Property of Eu^{2+}, Mn^{2+} Co-Doped Silicates Phosphors for White LED[J]. *J. Alloys Compd*., 2015, 632 756-632 759

[13] Zhang Y, Feng J, Sai Q, *et al*. Sol-Gel Synthesis and Photoluminescence Characterization of Ba_2SiO_4: Eu^{2+} Green Phosphors for White-LED Application[J]. *Integr. Ferroeletrics*, 2014, 154(1): 128-134

[14] Bobkova N and Trusova E. Glass-Ceramic Light-Converting Composites for Lighting Sources of a Remote Type Based on Light-Emitting Diodes[J]. *Glass Phys. Chem.*, 2015, 41(3): 296-301

[15] Shur M S and Zukauskas R. Solid-State Lighting: Toward Superior Illumination[J]. *Proceedings of the IEEE*, 2005, 93(10): 1691-1703

[16] Yanagisawa T and Kojima T. Long-Term Accelerated Current Operation of White Light-Emitting Diodes[J]. *J. Lumin*., 2005, 114(1): 39-42

[17] Chen L, Chen X, Liu F, *et al*. Charge Deformation and Orbital Hybridization: Intrinsic Mechanisms on Tunable Chromaticity of $Y_3Al_5O_{12}$: Ce^{3+} Luminescence by Doping Gd^{3+} for Warm White LEDs [J]. *Scientific Reports*, 2015, 5: 11 514-11 530

[18] Sun J and Cui D. Synthesis, Structure, and Thermally Stable Luminescence of Dy^{3+}-Doped $Na_3YSi_2O_7$ Host Compound[J]. *J. Am. Chem. Soc.*, 2014, 97(3): 843-847

[19] Hench L and Kokubo T. *Properties of Bioactive Glasses and Glass-Ceramics*, *Handbook of Biomaterial Properties*[M]. Berlin: Springer, 2016

[20] Huang S and Gu M. Enhanced Luminescent Properties of Tb^{3+} Ions in Transparent Glass Ceramics Containing $BaGdF_5$ Nanocrystals[J]. *J. Non-Cryst. Solids*, 2012, 358(1): 77-80

[21] Li C and Su Q. A New Blue Phosphorescent Glass-Ceramic: Rare-Earth-Doped Calcium Aluminoborate[J]. *J. Alloys Compd.*, 2006, 408 875-408 878

[22] Liu G, Zhou Z, Shi Y, *et al*. Ce: YAG Transparent Ceramics for Applications of High Power LEDs: Thickness Effects and High Temperature Performance[J]. *Mater. Lett.*, 2015, 139 480-139 482

[23] Chen D and Chen Y. Transparent Ce^{3+}: $Y_3Al_5O_{12}$ Glass Ceramic for Organic-Resin-Free White-Light-Emitting Diodes[J]. *Ceram. Int.*, 2014, 40(9): 15 325-15 329

[24] Chen L-Y, Cheng W-C, Tsai C-C, *et al*. High-Performance Glass Phosphor for White-Light-Emitting Diodes Via Reduction of Si-Ce^{3+}: YAG Inter-Diffusion[J]. *Opt. Mater. Express*, 2014, 4(1): 121-128

[25] Lee J S, Arunkumar P, Kim S, *et al*. Smart Design to Resolve Spectral Overlapping of Phosphor-in-Glass for High-Powered Remote-Type White Light-Emitting Devices[J]. *Optics Letters*, 2014, 39(4): 762-765

[26] Zhang R, Lin H, Yu Y, *et al*. A New-Generation Color Converter for High-Power White LED: Transparent Ce^{3+}: YAG Phosphor-in-Glass[J]. *Laser & Photonics Reviews*, 2014, 8(1): 158-164

[27] Su Y, Liu M, Han D, *et al*. Ce^{3+} and Ln^{3+} (Ln= Dy, Eu, Sm, Tb) Codoped SrF_2 Nanoparticles: Synthesis and Multicolor Light Emission[J]. *J. Nanosci. Nanotechnol*., 2016, 16(4): 3 956-3 960

[28] Okada G, Ueda J, Tanabe S, *et al*. Samarium-Doped Oxyfluoride Glass-Ceramic as a New Fast Erasable Dosimetric Detector Material for Microbeam Radiation Cancer Therapy Applications at the Canadian Synchrotron[J]. *J. Am. Chem. Soc.*, 2014, 97(7): 2 147-2 153

[29] Fang J, You H, Chen J, *et al*. Memory Devices Based on Lanthanide (Sm^{3+}, Eu^{3+}, Gd^{3+}) Complexes[J]. *Inorg. Chem*., 2006, 45(9): 3 701-3 704

[30] Lakshminarayana G, Yang R, Qiu J, *et al.* White Light Emission from Sm^{3+}/Tb^{3+} Codoped Oxyfluoride Aluminosilicate Glasses under Uv Light Excitation[J]. *J. Phys. D: Appl. Phys*., 2008, 42(1): 015 414

[31] Li H, Wang Q, Zhang Z, *et al*. Influence of SrO to Al_2O_3 Ratio on Crystallization and Luminescent Properties of Glass-Ceramics[J]. *Wuhan Ligong Daxue Xuebao*, 2009, 31(22): 12-15

[32] Sung Y-M and Park J S. Sintering and Crystallization of ($SrO{\cdot}SiO_2$)-($SrO{\cdot}Al_2O_3{\cdot}2SiO_2$) Glass-Ceramics[J]. *J. Mater. Sci*., 1999, 34(23): 5 803-5 809

[33] Ratnakaram Y, Naidu D T, Kumar A V, *et al*. Influence of Mixed Alkalies on Absorption and Emission Properties of Sm^{3+} Ions in Borate Glasses[J]. *Physica B Condens. Matter*., 2005, 358(1): 296-307

[34] Pan Z, James K, Cui Y, *et al.* Terbium-Activated Lithium-Lanthanum-Aluminosilicate Oxyfluoride Scintillating Glass and Glass-Ceramic[J]. *Nucl. Instrum. Methods Phys. Res. A*, 2008, 594(2): 215-219

[35] Tanabe S, Hayashi H, Hanada T, *et al.* Fluorescence Properties of Er^{3+} Ions in Glass Ceramics Containing LaF_3 Nanocrystals[J]. *Opt. Mater.*, 2002, 19(3): 343-349

[36] Paßlick C, Johnson J and Schweizer S. Crystallization Studies on Rare-Earth Co-Doped Fluorozirconate-Based Glasses[J]. *J. Non-Cryst. Solids*, 2013, 37 133-37 136

[37] Fu F, Chen B, Shen L, *et al*. Multi-Channel Transition Emissions of Sm^{3+} in Lithium Yttrium Aluminum Silicate Glasses and Derived Opalescent Glass Ceramics[J]. *J. Alloys Compd*., 2014, 582 265-582 272

[38] Rasool S N, Moorthy L R and Jayasankar C. Spectroscopic Investigation of Sm^{3+} Doped Phosphate Based Glasses for Reddish-Orange Emission[J]. *Opt. Commun*., 2013, 311 156-311 162

[39] Lakshminarayana G, Yang R, Mao M, *et al*. Photoluminescence of Sm^{3+}, Dy^{3+}, and Tm^{3+}-Doped Transparent Glass Ceramics Containing CaF_2 Nanocrystals[J]. *J. Non-Cryst. Solids*, 2009, 355(52): 2 668-2 673